Understanding shale fracture network complexity in the laboratory

Aly Abdelaziz, Phyllis S. Wu
Department of Civil and Mineral Engineering, University of Toronto, Ontario, Canada

Mei Li (corresponding author; meili.li@mail.utoronto.ca)
Department of Civil and Mineral Engineering, University of Toronto, Ontario, Canada

Earl Magsipoc, Karl Peterson, Giovanni Grasselli
Department of Civil and Mineral Engineering, University of Toronto, Ontario, Canada

ABSTRACT: Hydraulic fracturing is a complex multi-physics process that involves coupling of fluid flow and rock deformation/fracturing. Particularly, the propagation of fluid-driven fractures is a competing process greatly influenced by rock fabric and in-situ stress. However, it remains unclear how rock fabric affects the failure mechanisms and contributes to the resulting fracture network. To understand this, an 80 mm Montney shale outcrop cube was hydraulically fractured in the laboratory under in-situ true triaxial stress conditions. The fractured sample was then digitally 3D reconstructed by merging high-resolution, high-contrast serial section images. In-depth observation of the digitally-reconstructed induced fracture-network revealed the formation of bedding-controlled horizontal fractures, opening against σ_2 instead of the theoretically expected σ_3. This suggests the key role played by the bedding planes in determining the trajectory of the fluid-driven fracture network. En-echelon fractures observed near the injection borehole are convincing evidence of possible shear failures associated with hydraulic fracturing.

Keywords: hydraulic fracturing, 3D imaging, serial section reconstruction, true triaxial testing, breakdown pressure, shut-in pressure.

1 INTRODUCTION

Since its first adoption as "Hydrafrac" process in 1947 (Clark 1949), hydraulic fracturing has revolutionized oil and gas extraction operations and became the key technology that has allowed to unlock those low permeability resources that have been developed for the past twenty years (Keshavarz et al. 2018). Irrespective of the completion method (open hole, plug and perf, or sliding sleeve), the ultimate goal for hydraulic fracturing is to achieve an optimized fracture geometry that maximizes the stimulated rock volume (SRV) and thus enhances production.

The first fundamentals behind hydraulic fracturing date back to Hubbert and Willis 1957, who considered a normal faulting system with the maximum (σ_H) and minimum horizontal (σ_h) stresses acting perpendicular to the vertical wellbore. However, they overlooked the strength of the rock mass in tension presuming it "a notoriously undependable quantity" and to be "reduced to zero" at depth due to its intersection with one or more open joint system. Regardless, the conditions associated with

their work was very constrictive and most analytical equations thereafter consider a vertical hole where the horizontal stresses acting on the hole are either in a normal fault regime, i.e., σ_H and σ_h act perpendicular to the trajectory of the hole or that a reverse/thrust fault regime is being fractured where σ_h is the least principal stress (σ_3). In both cases, fracture initiation and propagation would occur perpendicular to σ_3 at breakdown pressures equal to or less than the vertical overburden pressure (σ_v). The fracture trajectory would be vertical to the hole cross section in the normal faulting regime and horizontal in the reverse/thrust fault regime. In the event the breakdown pressure is greater than σ_v, the pressure parting phenomenon is also possible. This phenomenon signifies rock rupture, i.e., failure due to injection of fluid into a bedding plane, joint, or other structural weaknesses (Torrey 1951). This phenomenon is recognized in well acidizing operations (Clark 1949; Torrey 1951) and is characterized by a fracture that extends rapidly and for considerable distance away from the injection hole.

Efforts have been made in recent years to undertake hydraulic fracturing under true triaxial testing to establish the effects that the in-situ stress, as well as the presence of weakness planes, have on the initiation and overall trajectory of the fracture (Hou et al. 2018; Tan et al. 2017). However, these works do not discuss, in detail, the results of the individual test, breakdown pressure, shut-in pressure, and the impacts of the material's tensile strength on the reported results. The case presented in this work takes an in-depth look at the failure processes that occur when the hydraulic fracturing is performed in strike-slip stress conditions in a formation showing medium anisotropy in terms of its rock mechanics strength properties.

2 TESTING METHODOLOGY

In order to investigate the breakdown pressure and rock heterogeneity on fracture propagation, a true triaxial hydraulic fracturing experiment under in-situ stress regime is conducted. The sample used was sourced from an outcrop rock that, as verified via conodont biostratigraphy, is equivalent to the Montney shale formation (Zelazny et al. 2018). Post-test, the sample was imaged at a high spatial resolution and reconstructed into a 3D volume via serial section reconstruction to verify the geometry of the induced fractures.

2.1 True Triaxial testing

The true triaxial test experiment (TTT) was conducted at the Rock Fracture Dynamics Facility at the University of Toronto. The sample was an 80 mm cube, chamfered at its edges to approximately 1.5 mm deep. A 6.35 mm diameter, 44.45 mm deep hole was drilled at the center of the cube. After mini-packer installation, the downhole open cavity left for injection and fluid delivery was 5 mm long. The experiment mimics a single-stage horizontal open-hole hydraulic fracturing using a slickwater system, composed of surfactant, friction reducer, and biocide as the injection fluid. The injection fluid was pumped at a constant rate of 7 mL/min to match the pressure rate used in field operations. The cube was subjected to the reservoir strike-slip in-situ stress condition, estimated via simple 1D Mechanical Earth Model (MEM) (Abul Khair and Adams 2019), where σ_H was the maximum principal stress (σ_1) of 63 MPa, σ_v was the intermediate principal stress (σ_2) of 49 MPa, and σ_h=σ_3 was 43 MPa. The dimensional difference between the TTT platens and the face of the cube reduced the stresses in the cube to σ_H=σ_1 54.6 MPa, σ_v=σ_2 42.2 MPa, and σ_h=σ_3 37.7 MPa. Efforts were made during the initial cube preparation to ensure that the hole lain between the bedding planes, making the mini-wellbore parallel to the direction of σ_3 and along the strike of the bedding planes. The true triaxial machine has 6 independent actuators and accordingly the stresses were raised isostatically. The linear deformation between each two opposing faces was measured using three linear variable differential transformers (LVDT). More detailed information pertaining to this test setup and the mechanical properties of the tested sample can be found in (Abdelaziz et al. 2019), and information pertaining to the true triaxial system are found in (Young et al. 2012; Lombos et al. 2012). Of importance, the indirect tensile strength of the rock was measured to be 12.4 and 18.6 MPa in direction parallel ($\sigma_{t\parallel}$) and perpendicular ($\sigma_{t\perp}$) to bedding, respectively.

2.2 Serial Section Reconstruction

To image the generated fractures, the cube was three-dimensionally (3D) visualized using the serial-section reconstruction method (Li et al. 2022). Before serial sectioning, an epoxy mixed with greenish-yellow ultraviolet (UV) fluorescent dye was injected through the borehole into the connected voids. After it was cured, the same epoxy mixed with orange-red UV fluorescent dye was used to impregnate the cube from the surfaces. This two-stage epoxy process was designed to enable the classification of fractures connected and not connected to the injection hole. Later, acrylic rods that fluoresce red under UV exposure were fixed to the side of the cube by another epoxy coating, which provided shared spatial references for image registration. For serial sectioning, the cube was magnetically fixed onto a Computerized Numerical Control (CNC) surface grinder, and a digital single-lens reflex camera equipped with an aspherical wide-angle lens and a UV ring lamp was attached to the housing of the grinder's wheel. The cube was then iteratively ground and photographed, with each grinding cycle cleanly removing a 50 μm layer of rock followed by imaging the newly exposed surface under UV light. A total of 1560 images were collected from the serial grinding which were registered and segmented for 3D reconstruction and visualization of the fractures within. Additional details pertaining to the 3D reconstruction and visualization of this cube can be found in Wu 2023.

3 RESULTS AND CONCLUSIONS

The mechanical response of the sample, during the duration of the fluid injection (Figure 1), clearly depicts typical stages of an in-situ hydraulic fracturing operation: the processes of cavity filling, open hole pressurization until breakdown pressure, followed by unstable pressure relief, and fracture propagation. The pressure rise during the open hole pressurization is about 3.1 MPa/s which is similar to the pressure rise during in-situ injection. Injection fluid was noticed flowing out from the σ_H=σ_1 (Figure 1–Y-direction), and the test was ended when the fluid pressure reached a steady state. Some rock imperfections are seen in Figure 2 d.

Instances of significant pressure drop accompanied by substantial movement in the LVDTs, are depicted by orange bands in Figure 1, namely Zones (A), (B), and (C). Zone (A) marks the maximum (breakdown) pressure at 49.8 MPa followed by an abrupt drop to 22.0 MPa. At the first pressure drop instance in the time domain, the pressure raised to a peak and was enough to overcome the stresses around the wellbore forming the primary fracture (Figure 2 – Primary fracture). The release in pressure was accompanied by LVDT movement indicative of the fracture opening in the σ_1-σ_3 plane (Figure 1–X-direction), i.e., opening was against σ_2, which is counterintuitive to the dogmatic expectation that the opening should occur against σ_3. However, the opening against σ_2 could be easily explained by the fact that $\sigma_2 + \sigma_{t\parallel}$ is smaller than $\sigma_3 + \sigma_{t\perp}$ (Table 1).

Table 1. Stresses in the cube and around the wellbore.

Parameter	σ_1	σ_2	σ_3	$\sigma_{t\parallel}$	$\sigma_{t\perp}$	$\sigma_2 + 0.9*\sigma_{t\parallel} < \sigma_3 + 0.9*\sigma_{t\perp}$
Stress (MPa)	54.6	42.2	37.7	12.4	18.6	53.4 < 54.4

* 0.9 is the ratio between the direct and σ_t of shale (Perras and Diederichs 2014)

The closure movement recorded in the LVDT σ_2-σ_3 plane (Figure 1–Y-direction) would suggest the hypothesis that the primary fracture opening was accompanied by either (1) a geometrical shape change in the open hole section from a circle to slightly elliptical or (2) slight shearing movement (Figure 2 b – en-echelon fracture) that caused the fracture to shift and the aperture of the fracture to change. Hypothesis (1) is better associated with Zone (A) as the compression is more prominent in the top part of the cube and is almost negligible at the bottom of the cube, supported by the change in aspect ratio of the drilled hole deduced from the serial section images. Hypothesis (2) could explain a possible slip event caused by the secondary fractures at Zone (B) and Zone (C), supported by the opposing movement in the LVDT in Figure 1–Z-direction.

The duration between Zone (A) and Zone (B) is characterized by small drops in pressure (peak-to-valley) of about 1 to 6 MPa, where the maximum fluid pressure during that duration is 46 MPa

and the minimum is 39.7 MPa. It is hypothesized that these occurred as part of the fluid advancing through the sample trying to create new fluid pathways and change in tortuosity (Figure 2 c and e – Horst and Graben feature). It is worth noting that there were no significant responses from the LVDT in this duration. Similarly, the duration between Zone (B) and Zone (C) experienced a similar phenomenon with fluctuations between 46.2 MPa and 41.1 MPa.

The fluid pressure at Zone (B) and Zone (C) significantly dropped from 45.9 MPa to 37.7 MPa and from 43.7 MPa to 33.0 MPa, respectively, suggesting large stress relief in the system. This hypothesis is supported by movement in the LVDT, highly suggesting the formation of a secondary fracture and/or pathway (Figure 2 a, b, c, and e– Secondary fracture).

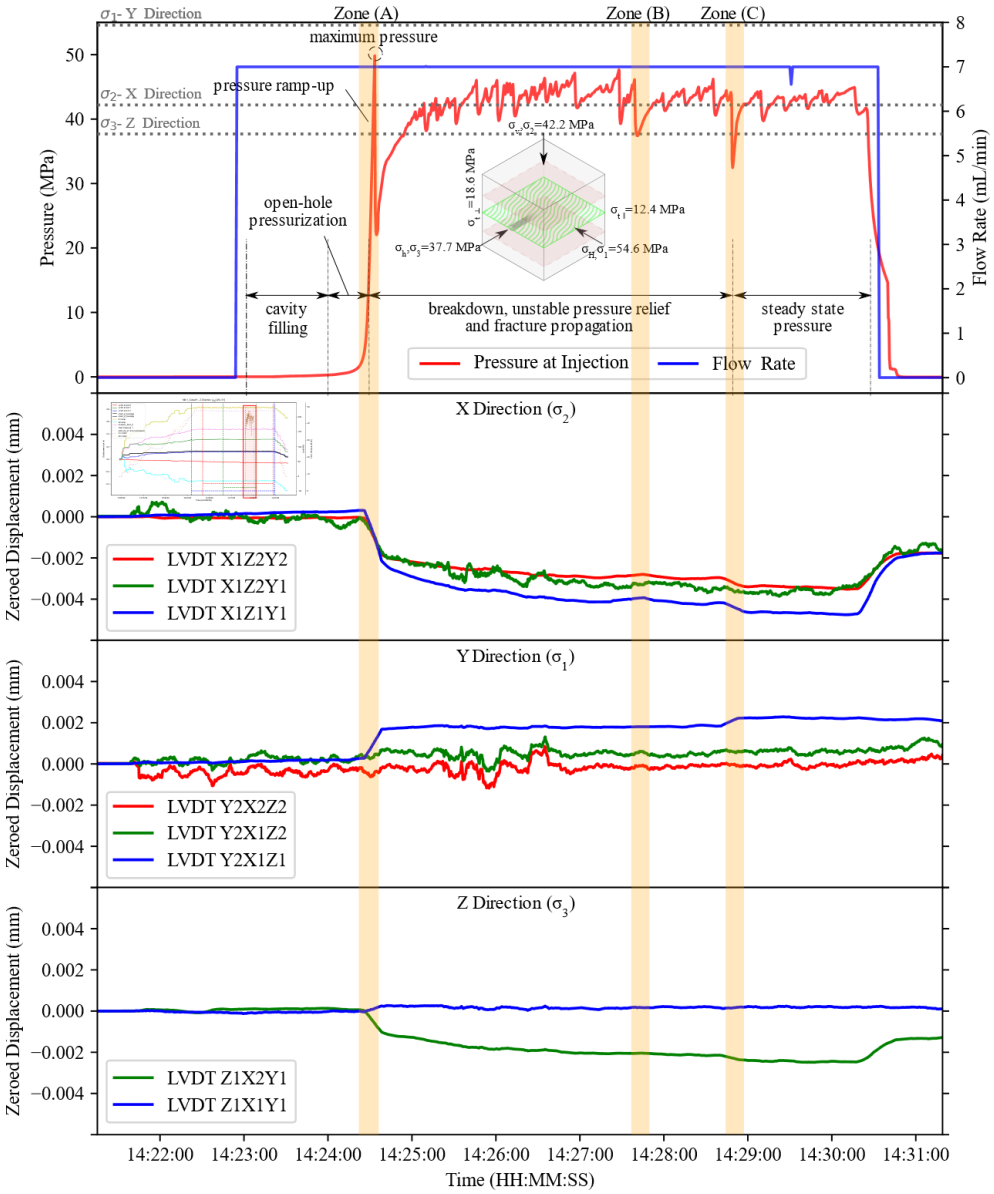

Figure 1. The injection flow rate, fluid pressure near the wellbore, and mechanical response of the LVDT's along the three principal axes during the duration of the fluid injection. The inset shows the total system response during the loading, fluid injection, and subsequent unloading. Negative LVDT movement indicates fracture opening. The orange bands indicate special areas of interest.

Beyond Zone (C), the drops in pressure became insignificant, i.e., about 1 to 2 MPa ranging from 43.5 MPa to 41.8 MPa, where it can be concluded that the hydraulic state within the cube reached a steady-state condition. Also, when steady-state was reached, the injection pressure stabilized at a

value equivalent to σ_2, i.e., the shut-in pressure where the stress is just enough to overcome the in-situ stress acting against the trajectory of the fracture and hold the hydraulic fracture open.

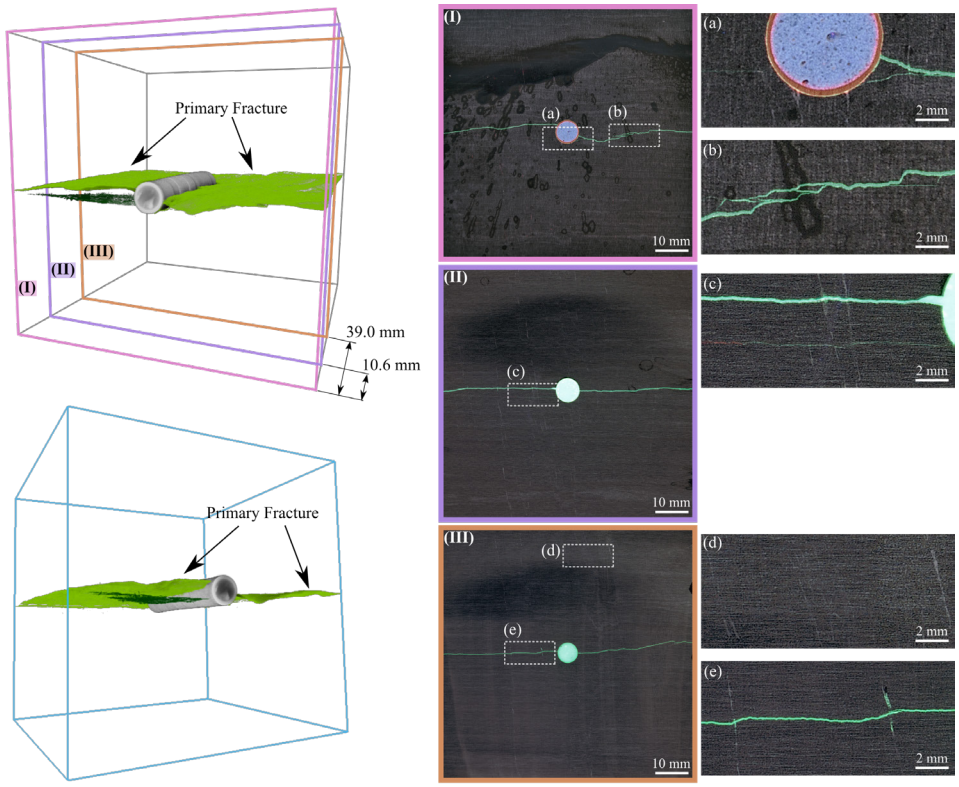

Figure 2. 3D reconstruction of the cube from serial sections. Cross-sections I-II-III from the cube indicating the various features within the reconstructed 3D image underlaid with the standard light image. a-e are zoom-in of views of areas of particular interest.

The results of the experiment clearly suggest that the initiation pressure of the hydraulic fracture, although influenced by the in-situ stress condition, is also equally influenced by the anisotropy of the rock matrix. In other words, the breakdown pressure required to overcome the stresses around the wellbore is a function of both the in-situ stress state and the anisotropy in the tensile strength of the rock material, both of which play an equally important role (i.e., the minimum of the in-situ principal stress and their associated tensile strength) and not necessarily limited to the magnitude of the principal stress (Table 1). The steady-state portion of the fluid pressure curve solidifies this hypothesis since the pressure needed to keep the fracture open is similar to the least of the above (i.e., $\sigma_2 + 0.9*\sigma_{t\,||}$) less the tensile strength as the tensile strength after fracturing goes to zero (Figure 1– grey horizontal lines).

The framework presented above reconstructs a 3D fracture network that is subsequent to the true triaxial hydraulic fracturing experiment that honored the in-situ stress regime and mimicked an open-hole completion. The results of the experiment, aided by the 3D visualization, depict the influential role that bedding planes and rock anisotropy have on the initiation pressure and trajectory of the hydraulic fracture. They also indicated that shearing may be occurring during the hydraulic fracturing process. Although the test induced a simple fracture, the results shed light on the dogma associated with hydraulic fractures being bi-wing and honoring their orientation to σ_3 and σ_3 being equal to the shut-in pressure. In this specific case, rock strength anisotropy favors initiation and propagation along the σ_1-σ_3 plane, i.e., opening against σ_2. In addition, the failure mechanism is assumed to be tensile-dominated and associated with a shear component at the microscale. Hence, the role of strength anisotropy of the rock mass should never be discounted during hydraulic fracturing operations.

ACKNOWLEDGEMENTS

This work has been supported through the Natural Sciences and Engineering Research Council of Canada (NSERC) PGS D3 - 518886, NSERC Discovery Grants 341275, NSERC/Energi Simulation Industrial Research Chair program, and Queen Elizabeth II GSST. The authors would like to acknowledge Petronas Canada for providing the outcrop samples; Dr. M.H.B Nasseri, Mr. Johnson Ha, and the Rock Fracture Dynamics Facility laboratory for their assistance in conducting the true triaxial test; and Mr. Yusheng Qiu for his advice and assistance during the epoxy impregnation.

REFERENCES

Abdelaziz, Aly; Ha, Johnson; Abul Khair, Hani; Adams, Matthew; Tan, Chee Phuat; Musa, Ikhwanul Hafizi; Grasselli, Giovanni (2019): Unconventional Shale Hydraulic Fracturing Under True Triaxial Laboratory Conditions, the Value of Understanding Your Reservoir. In : SPE Annual Technical Conference and Exhibition. Calgary, Alberta, Canada, September 2019.

Abul Khair, H.; Adams, M. (2019): Marrying seismic attributes and geomechanical analysis for de-risking induced seismicity in unconventional reservoirs. In : 2nd Asia Pacific Meeting on Near Surface Geoscience and Engineering. EAGE-GSM 2nd. Kuala Lumpur, Malaysia, Apr 2019.

Clark, J. B. (1949): A Hydraulic Process for Increasing the Productivity of Wells. In *Journal of Petroleum Technology* 1 (01), pp. 1–8. DOI: 10.2118/949001-G.

Hou, Bing; Zhang, Ruxin; Zeng, Yijin; Fu, Weineng; Muhadasi, Yeerfulati; Chen, Mian (2018): Analysis of hydraulic fracture initiation and propagation in deep shale formation with high horizontal stress difference. In *Journal of Petroleum Science and Engineering* 170 (2), pp. 231–243. DOI: 10.1016/j.petrol.2018.06.060.

Hubbert, M. King; Willis, David G. (1957): Mechanics of Hydraulic Fracturing. In *Transactions of the AIME* 210 (01), pp. 153–168. DOI: 10.2118/686-G.

Keshavarz, Alireza; Akhondzadeh, Hamed; Sayyafzadeh, Mohammad; Zargar, Masoumeh (2018): Enhanced Gas Recovery Techniques From Coalbed Methane Reservoirs. In Alireza Bahadori (Ed.): Fundamentals of Enhanced Oil and Gas Recovery from Conventional and Unconventional Reservoirs: Gulf Professional Publishing - Elsevier, pp. 233–268.

Li, Mei; Magsipoc, Earl; Abdelaziz, Aly; Ha, Johnson; Peterson, Karl; Grasselli, Giovanni (2022): Mapping Fracture Complexity of Fractured Shale in Laboratory. Three-dimensional Reconstruction From Serial-section Images. In *Rock Mech Rock Eng* 55 (5), pp. 2937–2948. DOI: 10.1007/s00603-021-02540-w.

Lombos, L; D.W. Roberts, D W; King, M S (2012): Design and development of integrated true triaxial rock testing system. In Marek Kwasniewski, Xiaochun Li, Manabu Takahashi (Eds.): True triaxial testing of rocks. 1st ed. London: CRC Press, pp. 35–51.

Perras, Matthew A.; Diederichs, Mark S. (2014): A Review of the Tensile Strength of Rock. Concepts and Testing. In *Geotech Geol Eng* 32 (2), pp. 525–546. DOI: 10.1007/s10706-014-9732-0.

Tan, Peng; Jin, Yan; Han, Ke; Hou, Bing; Chen, Mian; Guo, Xiaofeng; Gao, Jie (2017): Analysis of hydraulic fracture initiation and vertical propagation behavior in laminated shale formation. In *Fuel* 206 (2), pp. 482–493. DOI: 10.1016/j.fuel.2017.05.033.

Torrey, Paul D. (1951): Oil Recovery by Fluid Injection. In : 3rd World Petroleum Congress, WPC-4140. 3rd World Petroleum Congress. The Hague, the Netherlands, May 28–June 6, 1951: World Petroleum Congress, pp. 565–607.

Wu, Phyllis Shin-Yu (2023): Mechanical Properties of Outcropped Montney Shale. Master of Applied Science. University of Toronto, Ontario, Canada.

Young, R. P.; Nasseri, M. H.B.; Lombos, L. (2012): Imaging the effect of the intermediate principal stress on strength, deformation and transport properties of rocks using seismic methods. In Marek Kwasniewski, Xiaochun Li, Manabu Takahashi (Eds.): True triaxial testing of rocks. 1st ed. London: CRC Press, pp. 167–179.

Zelazny, Isabelle V.; Gegolick, Aimee; Zonneveld, John-Paul; Playter, Tiffany; Moslow, Thomas F. (2018): Sedimentology, stratigraphy and geochemistry of Sulphur Mountain (Montney equivalent) Formation outcrop in south central Rocky Mountains, Alberta, Canada. In *Bulletin of Canadian Petroleum Geology* 66 (1), pp. 288–317.